Ti (Zr)-Cu-Ni Bulk Metallic Glasses with Optimal Glass-Forming Ability and Their Compressive Properties

YAN-LING WANG and JIAN XU

The formation of bulk metallic glasses (BMGs) was systematically investigated in the ternary Ti-Cu-Ni and quaternary Ti-Zr-Cu-Ni systems. Over a relatively wide composition range (50 to 57 at. pct Ti, 34 to 44 at. pct Cu, and 6 to 10 at. pct Ni) in the ternary Ti-Cu-Ni system, new Ti-based BMGs with a critical diameter of 1 mm have been discovered in the triangular region enclosed by the three intermetallic compounds TiNi, TiCu, and Ti_2Cu. Partial substitution of Zr for Ti improved the glass-forming ability (GFA), and the BMGs of 3 mm in diameter were obtained in the composition range of 51 to 53 at. pct (Ti + Zr), 38 to 41 at. pct Cu, and 8 to 10 at. pct Ni. The enhanced GFA compared with the ternary Ti-Ni-Cu system was attributed to the effects of Zr on stabilizing the undercooled liquid. These Ti-based BMGs had compressive fracture strength higher than 2 GPa. Among them, the $Ti_{50}Cu_{43}Ni_7$ glass exhibited a reproducible plastic strain larger than 5 pct.

DOI: 10.1007/s11661-008-9647-6

I. INTRODUCTION

IN the family of bulk metallic glasses (BMGs), Ti-based glasses are of particular interest due not only to their high specific strength, good corrosion resistance, and relatively low cost, but also to their accessible plasticity during deformation.[1–6] However, compared with other BMG-forming systems based on common engineering metals such as Mg,[7,8] Cu,[9–12] and Fe,[13,14] the glass-forming ability (GFA) of Ti-based alloys is relatively low. The critical size (thickness or diameter) of the glass formation under copper mold casting, free of toxic elements such as Be, is no more than a few millimeters.[15–23] Consequently, it is necessary to further explore the GFA of Ti-based alloys without Be incorporation.

A majority of the previous studies on Ti-based BMG-forming systems have been focused on the Ti-Cu-Ni-based alloys, based on the criteria that the GFA of alloys correlates with a large supercooled liquid region, ΔT_x ($\Delta T_x = T_x - T_g$, where T_x and T_g are the onset temperature of crystallization and the calorimetric glass transition temperature, respectively).[15–19] This ternary system has been used as the compositional basis for the development of Ti-based BMGs with additional alloying elements.[17,18,24,25] However, studies on the BMG-forming composition range in the Ti-Cu-Ni base system remain incomplete, especially when considering that GFA has a strong dependence on the composition.[26,27] Therefore, it is important to conduct further systematic experiments to discover the full potential of the base ternary system, by locating the optimized glass-forming compositions before expanding the search into multi-component systems.

On the other hand, for a given quaternary system, it is possible in many cases to miss the optimal glass-forming composition when just using a simple substitution of a chemically-similar component based on the ternary alloys.[7,28] As a matter of fact, it has been indicated that before uncovering the full potential of the GFA in a given quaternary system, it is impossible to judge whether the effect of additional alloying elements on the GFA improvement is positive or negative.[28] Furthermore, a full determination of the optimized glass-forming composition in a given ternary/quaternary system will be useful for composition tailoring to develop ductile BMGs, because the mechanical properties of BMGs are also composition-dependent.[29–31]

In our previous work, new BMGs were found near the pseudo-binary eutectic ($L \rightarrow$ TiCu + TiNi) composition in the Ti-Cu-Ni ternary system. The best glass former was determined to be $Ti_{50}Cu_{43}Ni_7$, where glassy rods 1.5 mm in critical diameter (D_c) could be fabricated using the copper mold casting method.[32] The TiCu-TiNi eutectic is selected because TiNi has a less-dense packed B2 structure (a = 0.3015 nm).[33] In such a B2-phase-containing system, BMGs are more likely to be ductile because some B2 intermetallics can be ductile.[34,35] In the current work, we expand the search into the entire triangular compositional region enclosed by three compounds TiNi, TiCu, and Ti_2Cu in the Ti-Cu-Ni ternary system. Based on the best glass former, the fourth element Zr is added to partially substitute for Ti to form the Ti-Zr-Cu-Ni quaternary system. By adopting the "3D pinpointing approach" developed by our research team,[7,28,36] which has been extended to several quaternary systems based on Mg,[7,8,37] Cu,[10,12] Ni,[38] and Hf,[39] we have located new BMGs with a critical diameter of 3 mm. The

YAN-LING WANG, Postdoctoral Researcher, and JIAN XU, Professor, are with the Shenyang National Laboratory for Materials Science, Institute of Metal Research, Chinese Academy of Sciences, 72 Wenhua Road, Shenyang, 110016, China. Contact e-mail: jianxu@imr.ac.cn

Manuscript submitted March 5, 2008.
Article published online October 1, 2008

mapping was done at a 1 at. pct interval to capture the strong composition dependence of GFA. Moreover, these monolithic Ti-based BMGs are found to exhibit visible plastic deformability under compression loading.

II. EXPERIMENTAL

The master alloy ingots with nominal compositions (in at. pct) were prepared by arc melting the elemental pieces with purity better than 99.9 wt pct under a Ti-gettered argon atmosphere in a water-cooled copper crucible. The alloy ingots were melted several times to ensure compositional homogeneity. Cylindrical rod alloys of about 20 mm in length and 1 to 3 mm in diameter were produced using copper mold suction casting in a mini-arc melter.

The as-cast rods and arc-melted ingots were sectioned transversely and polished for X-ray diffraction (XRD) analysis and scanning electron microscopy (SEM) with energy dispersive X-ray (EDX) analysis. The XRD analysis was performed using a Rigaku D/max 2400 diffractometer (Tokyo, Japan) with monochromated Cu K_α radiation. The SEM observation of the samples was carried out in a LEO Supra 35 scanning electron microscope (Heidenheim, Germany).

The glass transition and crystallization temperatures of the as-cast BMG samples were determined in a Perkin-Elmer differential scanning calorimeter (Diamond-DSC, Shelton, CT) under flowing purified argon. A heating rate of 40 K min^{-1} was employed. To confirm the reproducibility of the results, at least three samples were measured for each composition. All the T_g and T_{x1} (the onset temperature of crystallization) measurements were reproducible within an error of ±1 K. The heat of crystallization, ΔH_x, for the glassy phase was determined by integrating the area under the DSC curve. The melting behavior of the alloys was measured in a Netzsch 404 DSC (Bayern, Germany) with alumina container, using a heating rate of 20 K min^{-1}.

Compression test samples 2 mm in height were cut from the as-cast rods of 1 mm in diameter. The loading surfaces were polished to be parallel to an accuracy of less than 10 μm. Room-temperature uniaxial compression tests were performed at a strain rate of 1×10^{-4} s^{-1} using an Instron 8871 machine (Norwood, MA). At least seven samples were measured for each composition. The strain was determined from the platen displacement after correction for machine compliance.

III. RESULTS

A. *BMG-Forming Composition Zone in the Ternary Ti-Cu-Ni System*

Figure 1 presents the BMG-forming composition map for 1-mm-diameter as-cast rods. The selected triangular region is enclosed by the three compounds TiNi, TiCu, and Ti_2Cu. The BMG-forming compositions for D_c = 1 mm fall within the region of 50 to 57 at. pct Ti, 34 to 44 at. pct Cu, and 6 to 10 at. pct Ni. Among them, alloys with the best GFA were located at $Ti_{50}Cu_{43}Ni_7$ and $Ti_{53}Cu_{39}Ni_8$, where the D_c reached 1.5 mm, as marked using stars in Figure 1. As shown in Figure 2(a), XRD patterns of these two as-cast rods with 1.5-mm-diameter exhibit broad halos in the 2θ = 35 to 50 deg range, characteristic of an amorphous phase. The corresponding DSC curves are shown in Figure 2(b). All curves exhibit an endothermic reaction associated with the glass transition, followed by the extended supercooled liquid region, and then two exothermic reactions due to crystallization. In terms of the crystallization behavior, the BMG-forming compositional zone is divided into two regions, I and II, as shown in Figure 1. The crystallization of BMGs in zone I proceeds through two steps, whereas three-step crystallization was observed in zone II, as illustrated in an inset in Figure 2 for 1-mm-diameter BMG of $Ti_{55}Cu_{36}Ni_9$ as a representative within this zone. The T_g and T_{x1} are marked by arrows in the DSC curves. With increasing Ti content from 50 to 55 at. pct, both T_g and T_{x1} decrease from 667 to 652 K and from 704 to 692 K, respectively, while the second crystallization peak shifts to higher temperature. The T_g, T_{x1}, ΔT_x, and ΔH_x for these ternary BMGs are listed in Table I.

To identify the crystalline phases competing with BMG formation, the microstructures of arc-melted alloys in weight of 20 g for the there ternary $Ti_{50}Cu_{43}Ni_7$, $Ti_{53}Cu_{39}Ni_8$, and $Ti_{55}Cu_{36}Ni_9$ alloys were observed using SEM in backscattered electron mode, as displayed in Figures 3(a) through (c), respectively. The chemical composition of the regions with different contrast was checked using EDX. Also, the corresponding XRD patterns of the arc-melted alloys are shown in Figure 4. The crystalline phases formed in these arc-melted alloys, determined based on the XRD results combined with the EDX analysis, are TiNi, TiCu, and Ti_2Cu

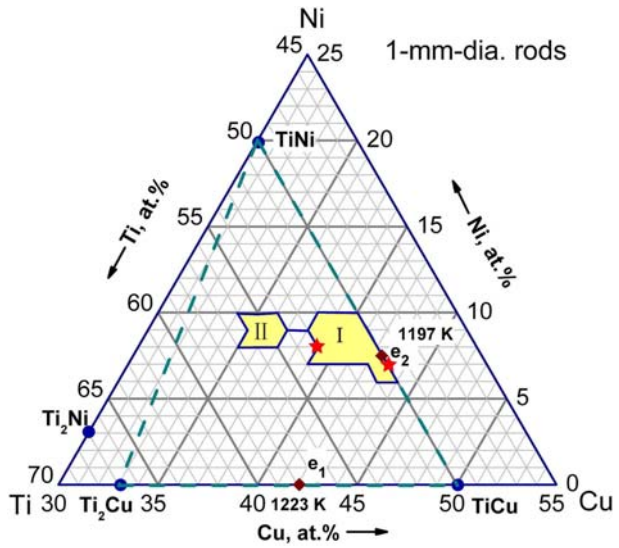

Fig. 1—BMG formation composition zone with D_c = 1 mm in the ternary Ti-Cu-Ni system. $Ti_{50}Cu_{43}Ni_7$ and $Ti_{53}Cu_{39}Ni_8$ with D_c = 1.5 mm are marked as starts. e_1 and e_2 are denoted by diamond symbols, representing the binary and pseudo-binary eutectic points, respectively. The assumed tie-lines between the compounds are drawn as the dashed lines.

intermetallics. Note that, with increasing Ti, the intensity of the Ti_2Cu diffraction peaks becomes stronger, indicating more volume fraction of this phase. These results confirm that the compositions we studied indeed reside in the region enclosed by the three compounds TiNi, TiCu, and Ti_2Cu.

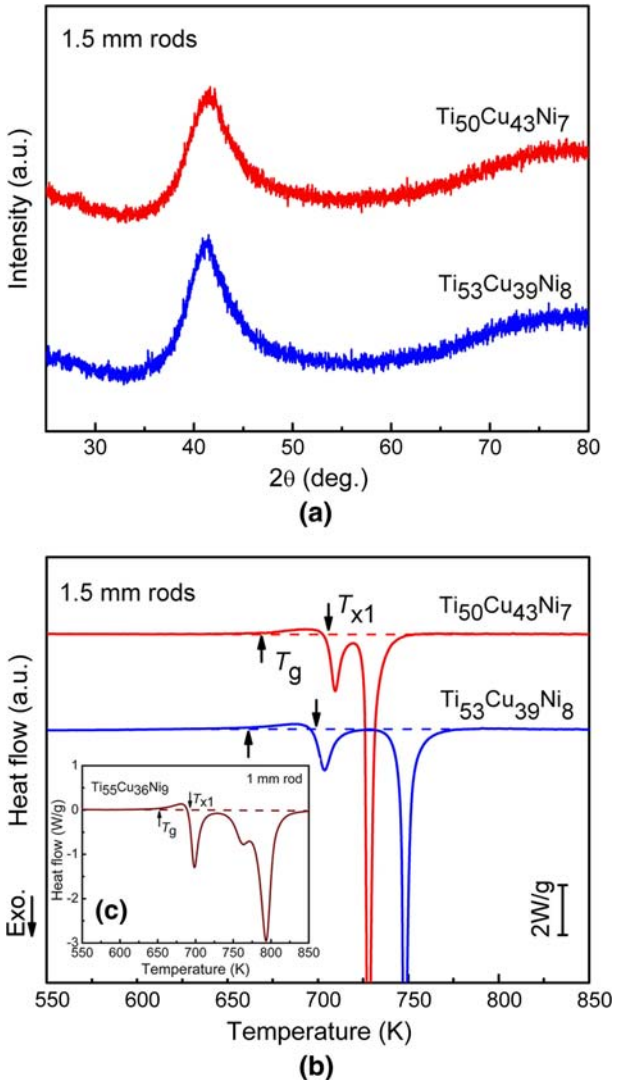

Fig. 2—(*a*) XRD patterns taken from the cross-sectional surface; (*b*) DSC scans, of as-cast ternary $Ti_{50}Cu_{43}Ni_7$ and $Ti_{53}Cu_{39}Ni_8$ BMGs with D_c = 1.5 mm; and (*c*) a DSC curve of $Ti_{55}Cu_{36}Ni_9$ BMG with D_c = 1 mm as a representative in the composition zone II.

Figure 5 shows the DSC curves during the heating and cooling runs near and above the melting temperature for the representative ternary BMG-forming alloys. The curves for the ternary $Ti_{53}Cu_{39}Ni_8$ and $Ti_{55}Cu_{36}Ni_9$ show at least two events, indicating that these alloys are at off-eutectic compositions. The T_m value (1197 K) corresponds to the pseudo-binary eutectic temperature for the reaction of $L \rightarrow$ TiCu + TiNi.[40] The T_m, T_L, and the calculated reduced glass transition temperature, T_{rg} ($T_{rg} = T_g/T_L$), of these alloys are also listed in Table I. The T_{rg} values of $Ti_{53}Cu_{39}Ni_8$ and $Ti_{55}Cu_{36}Ni_9$ alloys are 0.539 and 0.582, respectively, even though their GFAs are nearly the same. This finding indicates that a difference in T_{rg} does not directly reflect a difference of GFA in this system.

B. *Locating the Optimal BMG-Forming Composition for the Quaternary Ti-Zr-Cu-Ni Alloys*

Starting from the best ternary BMG former $Ti_{53}Cu_{39}Ni_8$ with D_c = 1.5 mm, Zr was selected to partially substitute for Ti to enhance the GFA. The Ti-Zr-Cu-Ni quaternary was treated as the (Ti, Zr)-Cu-Ni pseudo-ternary system. The optimal BMG-forming composition was investigated using the "3D pinpointing approach." Several consecutive compositional planes were examined, each with a fixed Zr to Ti ratio expressed as $Ti_{1-x}Zr_x$ (x = 0.1, 0.13, 0.15, 0.17). Figures 6(a) and (b) display the BMG-forming composition maps for as-cast rods with D_c = 2 mm (x = 0.1) and D_c = 3 mm (x = 0.15), respectively. The optimal ratio of Zr to Ti for BMG formation is located at x = 0.15. As illustrated in Figure 6(b), BMGs with D_c = 3 mm are found in the composition range of 51 to 53 at. pct (Ti + Zr), 38 to 41 at. pct Cu, and 8 to 10 at. pct Ni. On this compositional plane, at least five compositions were found to have nearly equivalent GFAs (D_c = 3 mm). It indicates that the partial substitution of Zr for Ti has effectively improved the GFA, increasing the D_c from 1.5 to 3 mm. In fact, it should be noted that this D_c is larger than many other "Ti-based" glasses.[19] For these quaternary BMGs, the Ti molar fraction is higher than that of Cu and higher than some other previously discovered "Ti-based" BMGs with D_c = 3 mm.[18,19]

Table I. Critical Diameter and Thermal Properties Measured with DSC for Ti(Zr)-Cu-Ni BMGs Fabricated Using Copper Mold Casting

Composition	D_c (mm)	T_g (K)	T_{x1} (K)	ΔT_x (K)	ΔH_x (kJ/mol)	T_m (K)	T_L (K)	T_{rg}
$Ti_{50}Cu_{43}Ni_7$	1.5	667	704	37	8.86	—	—	—
$Ti_{53}Cu_{39}Ni_8$	1.5	658	698	40	7.90	1197	1219	0.539
$Ti_{55}Cu_{36}Ni_9$	1	652	692	40	7.75	1198	1221	0.582
$Ti_{47.2}Zr_{5.8}Cu_{39}Ni_8$	2	665	700	35	6.30	—	—	—
$Ti_{47.2}Zr_{5.8}Cu_{38}Ni_9$	2	670	706	37	5.68	1110	1188	0.564
$Ti_{44.2}Zr_{7.8}Cu_{38}Ni_{10}$	3	664	708	44	5.10	1102	1189	0.561
$Ti_{44.2}Zr_{7.8}Cu_{39}Ni_9$	3	670	710	40	5.22	—	—	—
$Ti_{44.2}Zr_{7.8}Cu_{40}Ni_8$	3	669	702	33	5.45	—	—	—
$Ti_{45.05}Zr_{7.95}Cu_{39}Ni_8$	3	665	702	37	5.92	—	—	—
$Ti_{43.35}Zr_{7.65}Cu_{41}Ni_8$	3	660	705	45	4.78	—	—	—

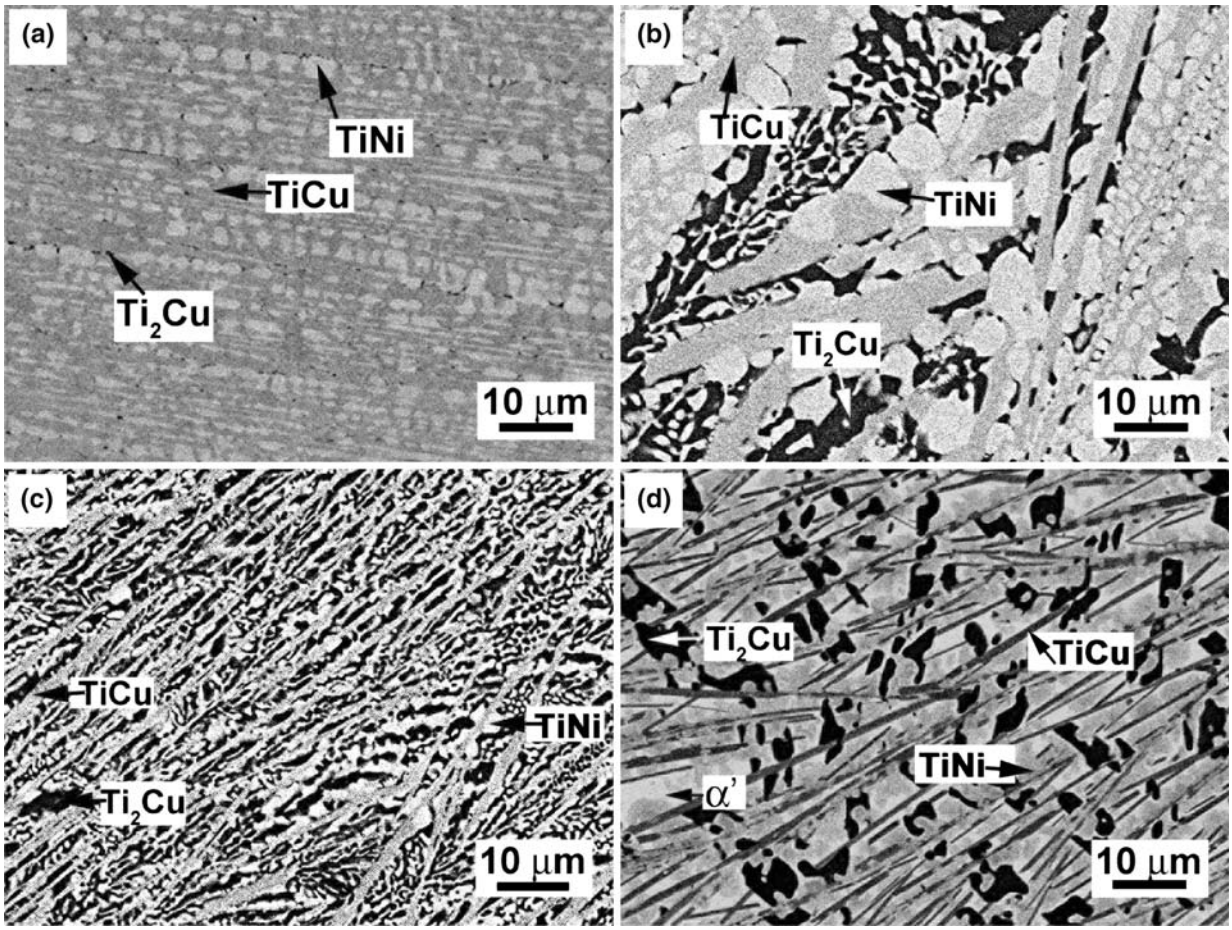

Fig. 3—Backscattered SEM images of the arc-melted alloys: (*a*) $Ti_{50}Cu_{43}Ni_7$, (*b*) $Ti_{53}Cu_{39}Ni_8$, (*c*) $Ti_{55}Cu_{36}Ni_9$, and (*d*) $Ti_{45.05}Zr_{7.95}Cu_{39}Ni_8$.

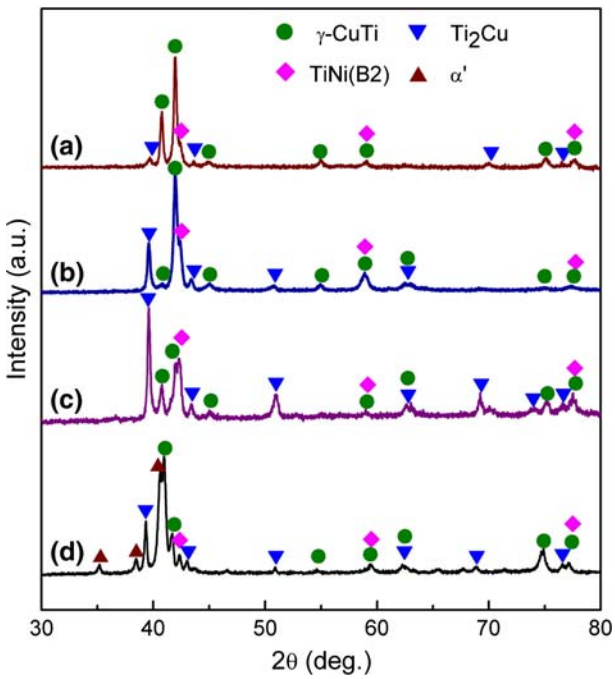

Fig. 4—XRD patterns of the arc-melted alloys: (*a*) $Ti_{50}Cu_{43}Ni_7$, (*b*) $Ti_{53}Cu_{39}Ni_8$, (*c*) $Ti_{55}Cu_{36}Ni_9$, and (*d*) $Ti_{45.05}Zr_{7.95}Cu_{39}Ni_8$.

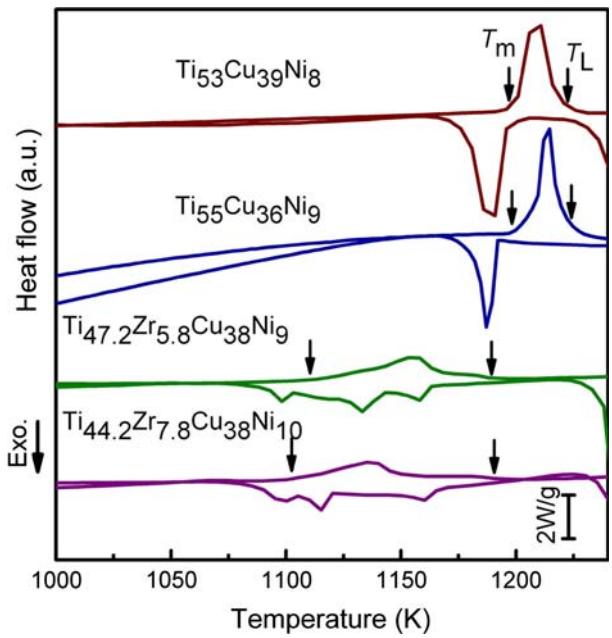

Fig. 5—DSC scans during the heating and cooling runs for the ternary $Ti_{53}Cu_{39}Ni_8$ and $Ti_{55}Cu_{36}Ni_9$ and the quaternary $Ti_{47.2}Zr_{5.8}Cu_{38}Ni_9$ and $Ti_{44.2}Zr_{7.8}Cu_{38}Ni_{10}$ BMG-forming alloys near their melting temperatures.

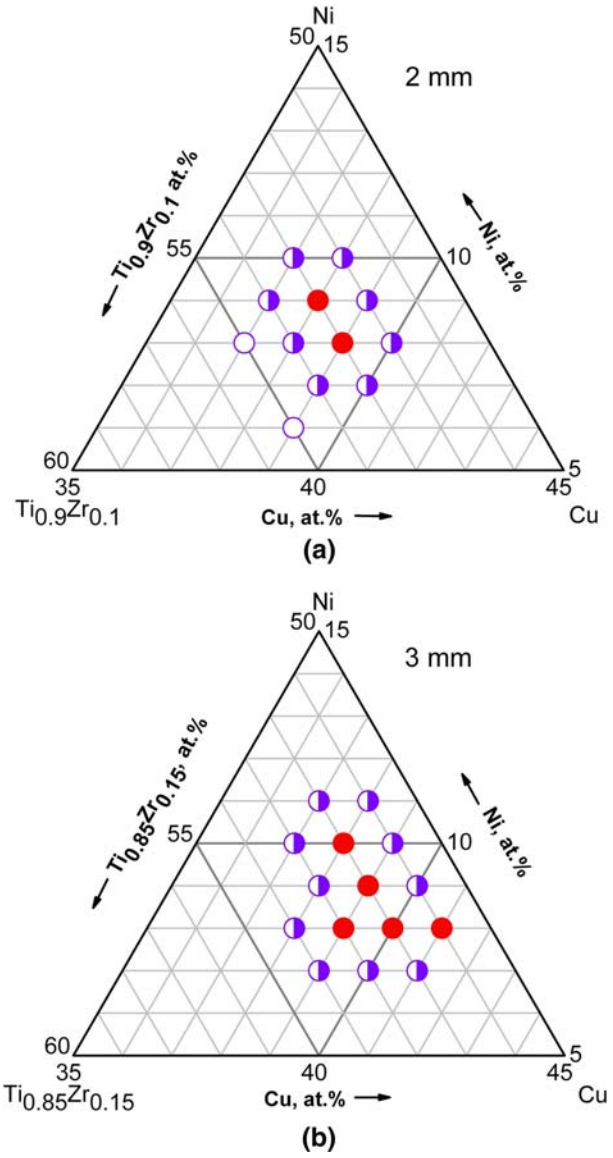

Fig. 6—Composition maps of BMG formation in the $(Ti_{1-x}Zr_x)$-Cu-Ni system. The two panels, (*a*) and (*b*), show the BMG-forming composition ranges at two ratios of $Ti_{1-x}Zr_x$, (a) $x = 0.1$ and (b) $x = 0.15$, for the as-cast rods of 2 and 3 mm in diameter, respectively.

Figures 7(a) and (b) display XRD patterns and DSC scans of five as-cast BMGs with a ratio of $Ti_{0.85}Zr_{0.15}$. The XRD patterns indicate that these 3-mm as-cast rods are fully glassy within the XRD resolution. As shown in Figure 7(b), the corresponding DSC curves display an endothermic reaction associated with the glass transition. In all cases, the crystallization process of the glassy phase is complex, characterized by multiple exothermic peaks, significantly different from the Ti-Cu-Ni ternary glasses (Figure 2(b)). Thermal properties measured from the DSC curves including the T_{x1}, ΔT_x, and ΔH_x for the representative quaternary BMGs are listed in Table I as well. Among these glasses, $Ti_{43.35}Zr_{7.65}Cu_{41}Ni_8$ exhibits the largest ΔT_x value about 45 K. The ΔT_x value of some quaternary

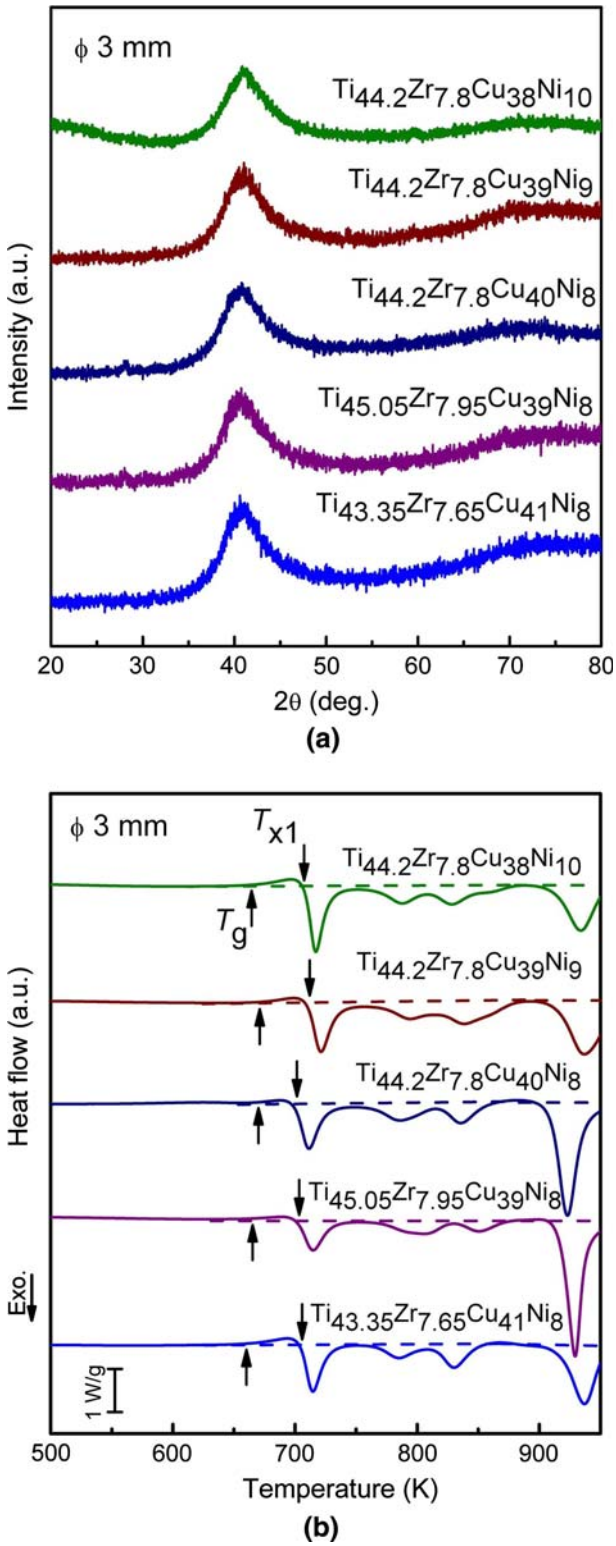

Fig. 7—(*a*) XRD patterns and (*b*) DSC scans of the as-cast rods of 3 mm in diameter for several $(Ti_{0.85}Zr_{0.15})$-Cu-Ni BMG-forming alloys.

BMGs with a higher GFA is even smaller than that of the ternary alloy. This finding implies that the ΔT_x value cannot exactly correlate with the difference in the GFA for these alloys. Then, it is impossible to locate

the optimal glass-forming composition using this guideline, as in previous studies.[15–19]

The DSC scans around the melting temperatures for the representative quaternary BMG alloys at $x = 0.1$ ($Ti_{47.2}Zr_{5.8}Cu_{38}Ni_9$) and $x = 0.15$ ($Ti_{44.2}Zr_{7.8}Cu_{38}Ni_{10}$) compositional planes are included in Figure 5 as well for comparison. Each of the curves for the quaternary alloys shows at least three events, indicating that these alloys are at off-eutectic compositions. Compared with the ternary alloys, with the addition of Zr, the onset melting temperature T_m and the liquidus temperature T_L (marked by arrows) significantly decreased, especially for T_m, by as much as 85 K for $Ti_{44.2}Zr_{7.8}Cu_{38}Ni_{10}$. This finding means that Zr addition leads to a significant stabilization of the liquid. The T_m, T_L, and T_{rg} of these alloys are also listed in Table I. The T_{rg} values of the quaternary alloys are around 0.56, consistent with their reasonable GFA to reach $D_c = 3$ mm.

The arc-melted $Ti_{45.05}Zr_{7.95}Cu_{39}Ni_8$ alloy was selected as a representative for the quaternary system to characterize the phase selection of the undercooled liquid during solidification at slow cooling rate. Its microstructure under SEM observation is shown in Figure 3(d) for comparison with the Zr-free ternary alloy. In the image, four phases with different contrasts are observed, which is evidently different from the case of the ternary alloys (Figures 3(a) through (c)). Furthermore, the XRD pattern for this alloy, as shown in Figure 4(d), indicates the presence of a hexagonal α' phase, which was identified also in other chill-cast TiZrCuNi-based alloys,[41] in addition to the TiNi, TiCu, and Ti_2Cu phases present in the ternary (Figures 4(a) through (c)). Combined with EDX analysis, the crystalline phase with bright contrast, as shown in Figure 3(d), can be identified to be the α' phase, which is enriched in Zr (37 at. pct Ti, 17 at. pct Zr, 39 at. pct Cu, and 7 at. pct Ni). This finding indicates that more crystalline phases than in the ternary case are involved in the Zr-containing quaternary alloy during crystallization of undercooled melt upon cooling. This adds difficulty to solute partitioning and coupled growth during crystallization, promoting the glass formation with respect to the ternary case.

C. *Compressive Properties of Ti(Zr)-Cu-Ni BMGs*

Figure 8 shows the room-temperature uniaxial compressive engineering stress-strain curves of three monolithic BMGs, including the ternary $Ti_{50}Cu_{43}Ni_7$ and $Ti_{53}Cu_{39}Ni_8$ ($D_c = 1.5$ mm) and the quaternary $Ti_{44.2}Zr_{7.8}Cu_{38}Ni_{10}$ ($D_c = 3$ mm). It is observed that, in all cases, fracture occurs after yielding, accompanied by visible plastic strain, indicating that deformation and fracture are controlled by localized shear bands rather than as-cast flaws in the samples. The fracture strength, σ_f, of the $Ti_{50}Cu_{43}Ni_7$, $Ti_{53}Cu_{39}Ni_8$, and $Ti_{44.2}Zr_{7.8}Cu_{38}Ni_{10}$ glasses are 2050 ± 60 MPa, 2160 ± 46 MPa, and 2230 ± 52 MPa, respectively. The TiZrCuNi quaternary BMG exhibits the σ_f significantly higher than that of TiCuNi ternary. The plastic strain ε_p of ternary $Ti_{50}Cu_{43}Ni_7$ glass was measured to be 5 to 11 pct. It should be emphasized that such plasticity is reproducible

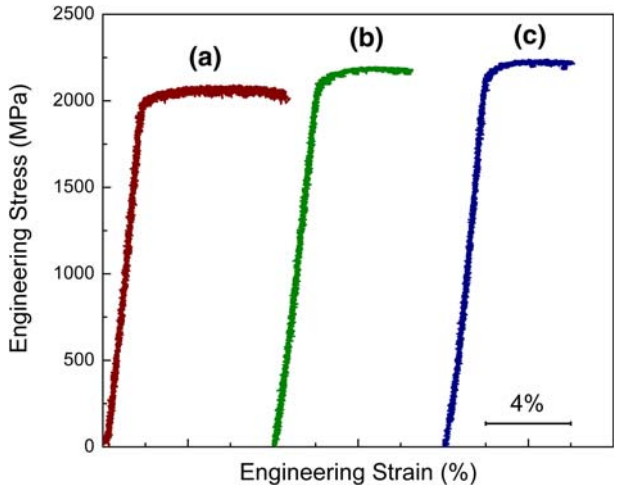

Fig. 8—Compressive engineering stress-strain curves for the as-cast BMGs with 1-mm diameter: ternary (*a*) $Ti_{50}Cu_{43}Ni_7$ and (*b*) $Ti_{53}Cu_{39}Ni_8$ and quaternary (*c*) $Ti_{44.2}Zr_{7.8}Cu_{38}Ni_{10}$. The curves are shifted relative to each other for clarity.

in almost all tested samples. In our case, the test samples were carefully prepared to rule out the "apparent plasticity" caused by sample miscut leading to deviation from orthogonality[42] and by interlock between the fractured parts.[43] However, the ε_p of the ternary $Ti_{53}Cu_{39}Ni_8$ and quaternary $Ti_{44.2}Zr_{7.8}Cu_{38}Ni_{10}$ glass is scattered within 0 to 6 pct and 0 to 5 pct, respectively.

IV. DISCUSSION

Our analysis indicates that the Ti-Cu-Ni ternary alloys we studied are located in a region enclosed by the three compounds TiNi, TiCu, and Ti_2Cu (not TiNi, TiCu, and Ti_2Ni or others). The T_m (1197 K) of the ternary alloys $Ti_{53}Cu_{39}Ni_8$ and $Ti_{55}Cu_{36}Ni_9$ corresponds to the melting of a pseudo-eutectic of $L \rightarrow$ TiCu + TiNi, exhibiting a eutectic temperature 26 K lower than the eutectic ($L \rightarrow$ TiCu + Ti_2Cu) in the Ti-Cu binary subsystem.[44] Evidently, the high GFA of these alloys relates to the deep eutectic feature of the system. The finding that $Ti_{53}Cu_{39}Ni_8$ alloy has nearly equivalent GFA ($D_c = 1.5$ mm) with $Ti_{50}Cu_{43}Ni_7$ suggests that there can be more than one optimum glass-forming composition within a given eutectic system.

Compared with the ternary $Ti_{53}Cu_{39}Ni_8$, the present results clearly show that Zr partially substituting for Ti can improve the GFA. The results of microstructure and XRD studies of the Zr-containing quaternary alloy, when compared with those for the base ternary, demonstrate that introduction of Zr does not eliminate (or change) any of the three competing crystalline phases corresponding to the ternary $Ti_{53}Cu_{39}Ni_8$. However, the Zr effect on lowering the liquidus and solidus temperatures is remarkable. This evident stabilization of the liquid state is believed to be the main factor contributing to the improved GFA of the quaternary alloys. The reasons are twofold. First, the heat of mixing in the liquid state between the Ni-Zr and Cu-Zr pairs is −49 and −23 kJ/mol, respectively, significantly

larger than that of the Ni-Ti (−35 kJ/mol) and Cu-Ti (−9 kJ/mol) pairs.[45] As a result, the enhanced atomic bonding helps to stabilize the clusters in the liquid. Second, there is also an atomic size difference between Ti (r_{Ti} = 0.146 nm) and Zr (r_{Zr} = 0.160 nm). This facilitates the formation of various local atomic clusters[46] and slows the atomic mobility needed for long-range partitioning of the constituent elements. These effects promote the stability of the amorphous structure, while retarding the formation of the competing crystalline phases during solidification. Compared with Ti-Ni, the Zr-Ni couple is known to be more likely to frustrate the competing compounds and reach the glassy state.[47]

As shown previously, the Ti(Zr)-Cu-Ni BMGs developed in the current work have a plasticity superior to other BMG systems, such as ZrCuAl[42] or CuZrAg,[31] let alone MgZnCa.[48] Obviously, such plasticity correlates with the intrinsic internal structure including short-range order, medium-range order, and excessive volume in the glasses. Recently, it has been revealed that the ductility of brittle amorphous steel can be improved by manipulating the electronic structure in the glasses.[49,50] The approach we adopted here to improve the ductility of BMGs is by selecting a eutectic system containing the B2 phase. Such intermetallics competing with glass formation are at least more ductile than those with a complex structure, such as Frank–Kasper structure (σ, Laves or μ phases).[34,35] For the latter phases, icosahedral clusters with a coordination number of 12 take a high volume fraction.[51] The alloy systems involving such structures can have a GFA higher than those containing phases with simple structures, but a lower ductility at the same time. Similar to our results, it has been found recently that the CuZr (B2)-containing system can be more ductile than others.[31] Further work is needed to systematically validate if indeed the structure of the competing intermetallics involved can be used as an indicator to develop new ductile BMGs, while maintaining a modest critical size.

V. CONCLUSIONS

We have systematically investigated the GFA in the ternary Ti-Cu-Ni system. A number of new BMGs with a critical diameter (D_c) of 1 mm under copper mold casting have been found. Based on the best ternary glass former $Ti_{53}Cu_{39}Ni_8$ with D_c = 1.5 mm, Zr was introduced to partially substitute for Ti to further improve the GFA. The best glass-forming alloys with D_c = 3 mm were discovered in the composition region of 51 to 53 at. pct (Ti + Zr), 38 to 41 at. pct Cu, and 8 to 10 at. pct Ni. The improvement in the GFA was attributed to the chemical and topological effects of Zr on stabilizing the liquid. These new Ti-based BMGs without Be element are interesting, because, compared with previously discovered ones, some of them have higher Ti content (up to 53 at. pct), higher GFA, or higher strength (up to 2230 MPa). Moreover, these Ti-based BMGs are also often ductile, unlike some other BMGs with similarly high specific strength.[48,52]

ACKNOWLEDGMENTS

The authors gratefully acknowledge the stimulating discussion with Professors E. Ma, Y. Li, and C. Suryanarayana. This research was supported by the National Natural Science Foundation of China under Contract No. 50871112 and the National Basic Research Program of China (973 Program) under Contract No. 2007CB613906.

REFERENCES

1. K.B. Kim, J. Das, X.D. Wang, X. Zhang, J. Eckert, and S. Yi: *Phil. Mag. Lett*., 2006, vol. 86, pp. 479–86.
2. G. Wang, Y.H. Liu, P. Yu, D.Q. Zhao, M.X. Pan, and W.H. Wang: *Appl. Phys. Lett*., 2006, vol. 89, pp. 251909-1–251909-3.
3. T. Ohkubo, D. Nagahama, T. Mukai, and K. Hono: *J. Mater. Res*., 2007, vol. 22, pp. 1406–13.
4. X.F. Zhang, K.B. Kim, J. Das, S. Yi, and J. Eckert: *J. Mater. Res*, 2007, vol. 22, pp. 2223–29.
5. J. Shen, Y.J. Huang, and J.F. Sun: *J. Mater. Res*., 2007, vol. 22, pp. 3067–74.
6. E.S. Park, H.J. Chang, J.Y. Lee, and D.H. Kim: *J. Mater. Res*., 2007, vol. 22, pp. 3440–47.
7. H. Ma, L.L. Shi, J. Xu, Y. Li, and E. Ma: *Appl. Phys. Lett*., 2005, vol. 87, pp. 181915-1–181915-3.
8. Q. Zheng, J. Xu, and E. Ma: *J. Appl. Phys*., 2007, vol. 102, pp. 113519-1–113519-5.
9. D.H. Xu, G. Duan, and W.L. Johnson: *Phys. Rev. Lett*., 2004, vol. 92, pp. 245504-1–245504-4.
10. C.L. Dai, H. Guo, Y. Shen, Y. Li, E. Ma, and J. Xu: *Scripta Mater*, 2006, vol. 54, pp. 1403–08.
11. P. Jia, H. Guo, Y. Li, J. Xu, and E. Ma: *Scripta Mater*., 2006, vol. 54, pp. 2165–68.
12. Y. Shen, E. Ma, and J. Xu: *J. Mater. Sci. Technol*., 2008, vol. 24, pp. 149–52.
13. Z.P. Lu, C.T. Liu, J.R. Thompson, and W.D. Porter: *Phys. Rev. Lett*., 2004, vol. 92, pp. 245503-1–245503-4.
14. V. Ponnambalam, S.J. Poon, and G.J. Shiflet: *J. Mater. Res*, 2004, vol. 19, pp. 1320–23.
15. T. Zhang and A. Inoue: *Mater. Trans. JIM*, 1999, vol. 40, pp. 301–06.
16. T. Zhang and A. Inoue: *Mater. Sci. Eng. A*, 2001, vols. 304–306, pp. 771–74.
17. C.L. Ma, S. Ishihara, H. Soejima, N. Nishiyama, and A. Inoue: *Mater. Trans*., 2004, vol. 45, pp. 1802–06.
18. C.L. Ma, H. Soejima, S. Ishihara, K. Amiya, N. Nishiyama, and A. Inoue: *Mater. Trans*., 2004, vol. 45, pp. 3223–27.
19. H. Men, S.J. Pang, A. Inoue, and T. Zhang: *Mater. Trans*, 2005, vol. 46, pp. 2218–20.
20. Y.J. Huang, J. Shen, J.F. Sun, and X.B. Yu: *J. Alloys Compd*, 2007, vol. 427, pp. 171–75.
21. F.Q. Guo, H.J. Wang, S.J. Poon, and G.J. Shiflet: *Appl. Phys. Lett*., 2005, vol. 86, pp. 091907-1–091907-3.
22. J.M. Park, Y.C. Kim, W.T. Kim, and D.H. Kim: *Mater. Trans*, 2004, vol. 45, pp. 595–98.
23. G. Duan, K.D. Blauwe, M.L. Lind, J.P. Schramm, and W.L. Johnson: *Scripta Mater*, 2008, vol. 58, pp. 465–68.
24. T. Zhang and A. Inoue: *Mater. Trans. JIM*, 1998, vol. 39, pp. 1001–06.
25. Y.C. Kim, S. Yi, W.T. Kim, and D.H. Kim: *Mater. Sci. Forum*, 2001, vols. 360–362, pp. 67–72.
26. D. Wang, Y. Li, B.B. Sun, M.L. Sui, K. Lu, and E. Ma: *Appl. Phys. Lett*, 2004, vol. 84, pp. 4029–31.
27. H. Ma, Q. Zheng, J. Xu, Y. Li, and E. Ma: *J. Mater. Res*, 2005, vol. 20, pp. 2252–55.
28. H. Ma, L.L. Shi, J. Xu, Y. Li, and E. Ma: *J. Mater. Res*, 2006, vol. 21, pp. 2204–14.
29. R.D. Conner and W.L. Johnson: *Scripta Mater*, 2006, vol. 55, pp. 645–48.
30. Y.H. Liu, G. Wang, R.J. Wang, D.Q. Zhao, M.X. Pan, and W.H. Wang: *Science*, 2007, vol. 315, pp. 1385–88.

31. G. Duan, K.D. Blauwe, M.L. Lind, J.P. Schramm, and W.L. Johnson: *Scripta Mater*, 2008, vol. 58, pp. 159–62.
32. Y.L. Wang, E. Ma, and J. Xu: *Phil. Mag. Lett*, 2008, vol. 88, pp. 319–25.
33. K.M. Knowles and D.A. Smith: *Acta Metall*, 1981, vol. 29, pp. 101–10.
34. K. Gschneidner, A. Russell, A. Pecharsky, J. Morris, Z.H. Zhang, T. Lograsso, D. Hsu, C.H. Chesterlo, Y.Y. Ye, A. Slager, and D. Kesse: *Nat. Mater*, 2003, vol. 2, pp. 587–91.
35. J. Morris, Y. Ye, M. Kremar, and C.L. Fu: *Mater. Res. Soc. Symp. Proc*, 2007, vol. 980, pp. 1106–10.
36. Y. Li, S.J. Poon, G.J. Shiflet, J. Xu, D.H. Kim, and J.F. Löffler: *MRS Bull*, 2007, vol. 32, pp. 624–28.
37. Q. Zheng, H. Ma, E. Ma, and J. Xu: *Scripta Mater*, 2006, vol. 55, pp. 541–44.
38. L. Zhang, M.J. Zhuo, and J. Xu: *J. Mater. Res*, 2008, vol. 23, pp. 688–99.
39. L. Zhang, E. Ma, and J. Xu: *Intermetallics*, 2008, vol. 16, pp. 584–86.
40. S.P. Alisova, N.V. Volynskaya, P.B. Budbery, and A.V. Kobylkin: in *Handbook of Ternary Alloy Phase Diagrams*, P. Villars, A. Prince, and H. Okamoto, eds., ASM INTERNATIONAL, Materials Park, OH, 1995, vol. 8, pp. 9846–61.
41. G. He, J. Eckert, and M. Hagiwara: *Mater. Lett*, 2006, vol. 60, pp. 656–61.
42. W.F. Wu, Y. Li, and C.A. Schuh: *Phil. Mag*, 2008, vol. 88, pp. 71–89.
43. K. Mondal, G. Kumar, T. Ohkubo, K. Oishi, T. Mukai, and K. Hono: *Phil. Mag. Lett*, 2007, vol. 87, pp. 625–35.
44. J.L. Murray: in *Binary Alloy Phase Diagram*, 2nd ed., T.B. Massalski, H. Okamoto, P.R. Subramanian, and L. Kacprzak, eds., ASM INTERNATIONAL, 1990, vol. 2, pp. 1494–96.
45. F.R. De Boer, R. Boom, W.C.M. Mattens, A.R. Miedema, and A.K. Niessen: *Cohesion in Metals*, North-Holland, Amsterdam, 1988.
46. H.W. Sheng, W.K. Luo, F.M. Alamgir, J.M. Bai, and E. Ma: *Nature*, 2006, vol. 439, pp. 419–25.
47. W.J. Meng, B. Fultz, E. Ma, and W.L. Johnson: *Appl. Phys. Lett*, 1987, vol. 51, p. 661.
48. Y.Y. Zhao, E. Ma, and J. Xu: *Scripta Mater*, 2008, vol. 58, pp. 496–99.
49. X.J. Gu, S.J. Poon, G.J. Shiflet, and M. Widom: *Acta Mater*, 2008, vol. 56, pp. 88–94.
50. H.J. Wang, X.J. Gu, S.J. Poon, and G.J. Shiflet: *Phys. Rev. B.*, 2008, vol. 77, pp. 014204-1–014204-8.
51. R. Ferro and A. Saccone: in *Structure of Intermetallc Compounds and Phases in Physical Metallurgy*, 4th revised and enhanced ed., R.W. Cahn and P. Haasen, eds., Elsevier Science B.V., Amsterdam, The Netherlands, 1996, p. 205.
52. Y.K. Xu, H. Ma, J. Xu, and E. Ma: *Acta Mater*, 2005, vol. 53, pp. 1857–66.